NANO LETTERS

pubs.acs.org/NanoLett
Letter

Plasmonic Diamond Membranes for Ultrafast Silicon Vacancy Emission

Andrew M. Boyce,[†] Hengming Li,[†] Nathaniel C. Wilson,[†] Deniz Acil, Amirhassan Shams-Ansari, Srivatsa Chakravarthi, Christian Pederson, Qixin Shen, Nicholas Yama, Kai-Mei C. Fu, Marko Loncar, and Maiken H. Mikkelsen*

Cite This: *Nano Lett.* 2024, 24, 3575−3580

ABSTRACT: Silicon vacancy centers (SiVs) in diamond have emerged as a promising platform for quantum sciences due to their excellent photostability, minimal spectral diffusion, and substantial zero-phonon line emission. However, enhancing their slow nanosecond excited-state lifetime by coupling to optical cavities remains an outstanding challenge, as current demonstrations are limited to ∼10-fold. Here, we couple negatively charged SiVs to sub-diffraction-limited plasmonic cavities and achieve an instrument-limited ≤8 ps lifetime, corresponding to a 135-fold spontaneous emission rate enhancement and a 19-fold photoluminescence enhancement. Nanoparticles are printed on ultrathin diamond membranes on gold films which create arrays of plasmonic nanogap cavities with ultrasmall volumes. SiVs implanted at 5 and 10 nm depths are examined to elucidate surface effects on their lifetime and brightness. The interplay between cavity, implantation depth, and ultrathin diamond membranes provides insights into generating ultrafast, bright SiV emission for next-generation diamond devices.

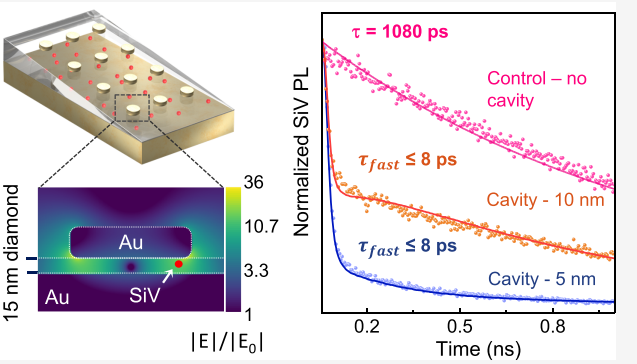

KEYWORDS: *plasmonics, nanocavity, silicon vacancy, diamond, Purcell enhancement*

Solid-state photon sources, such as quantum dots, defects in 2D materials, and color centers in diamond are critical components for quantum information and sensing technologies but are typically limited by their slow spontaneous emission rates and low photon extraction efficiencies.[1−3] Quantum emitters can function as gates in single photon transistors,[4] store and process quantum information,[5−7] and act as nanoscale temperature,[8,9] strain[10] and electromagnetic field sensors.[9,11,12] In particular, color centers in diamond, such as silicon vacancies and other group IV defects, are promising for practical applications due to their excellent photostability, accessible spin states, minimal spectral diffusion, and nearly lifetime-limited line widths.[1,13] However, emission rates from ordinarily dim diamond vacancy centers are limited by intrinsic lifetimes on the order of nanoseconds.[13,14] A promising approach to enhance their spontaneous emission rate is via the Purcell effect, in which the local density of states can be increased by embedding color centers in optical cavities,[15−18] where the degree of enhancement is proportional to the quotient of a cavity's quality factor (Q) and mode volume (V). Photonic crystal cavities leverage high Q with dimensions in the micrometer scale, in contrast to plasmonic nanogap cavities that target ultrasmall V in the nanometer regime to achieve high Purcell enhancement with lower Q. Further, nanoantenna effects enhance the absorption rate and therefore excitation efficiency, leading to greater emitter brightness.

Previous demonstrations of negatively charged silicon vacancy centers (SiVs) coupled to photonic crystal cavities have been limited to ∼10-fold lifetime reduction or less in patterned bulk diamond,[16,17] partly due to the diffraction-limited mode volumes of these approaches. Plasmonic cavities offer the advantage of sub-diffraction-limited mode volumes. A recent study demonstrated 70-fold enhancement of the spontaneous emission rate of negatively charged nitrogen vacancy (NV) centers in diamond nanocrystals.[19] However, achieving functional device integration can be nontrivial for diamond nanocrystals, as they suffer from random emitter dipole orientation, surface traps,[20] spectral diffusion from inhomogeneous local strains,[21] and degraded spin coherence times from paramagnetic defects.[22] Single crystal diamond

Received: October 17, 2023
Revised: February 16, 2024
Accepted: February 20, 2024
Published: March 13, 2024

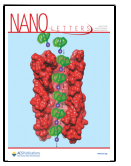

https://doi.org/10.1021/acs.nanolett.3c04002
Nano Lett. 2024, 24, 3575−3580

membranes offer a more controlled host for defect centers, with fixed dipole orientations, emitter depth control,[23,24] a larger physical extent which allows for strain tunability,[25] and overall improved integration potential.[26−29]

Here, we integrate SiVs in nanoscale thin film diamond with ultrasmall mode volume plasmonic nanogap cavities. The nanostructures are tailored to overlap the plasmon resonance with the SiV emission wavelength, resulting in a detector-limited 135-fold lifetime enhancement. Characterization of SiVs with 5 and 10 nm implantation depths reveals the depth effects on their brightness and lifetime, providing device design guidelines for near-term thin film diamond integration.

To control the local density of states of SiVs, diamond membranes with a varying thickness across each membrane are embedded into nanogap plasmonic cavities. First, SiVs are formed by ion implantation at either 5 or 10 nm depth in the diamond samples, followed by a high-temperature anneal and oxygen termination. Next, the diamond samples are inverted and thinned into membranes by reactive ion etching. Control samples are completed by transferring diamond membranes with 5 or 10 nm implantation depth onto a silicon substrate. Next, the nanocavity samples are fabricated by transferring diamond membranes, with implanted SiVs at either 5 or 10 nm depths, onto a gold film. , gold nanodisks are transferred on top of the gold-diamond stack using a PDMS-stamp as shown in Figure 1a−c, completing the nanogap cavities (details in SI).

Notably, the fabrication results in the implanted side facing the underlying Au ground plane. Therefore, the 5 and 10 nm implantation depths result in SiVs positioned approximately 5 and 10 nm above the ground plane. The final device schematic is illustrated in Figure 2a. The etching process produces a thin etched slab with a gradient of ∼2 nm/μm and a minimum thickness ranging from 10 to 20 nm. A height profile of the thinnest region is shown in Figure 2b and was measured using an imaging ellipsometer (Accurion nanofilm_ep4) (see SI).

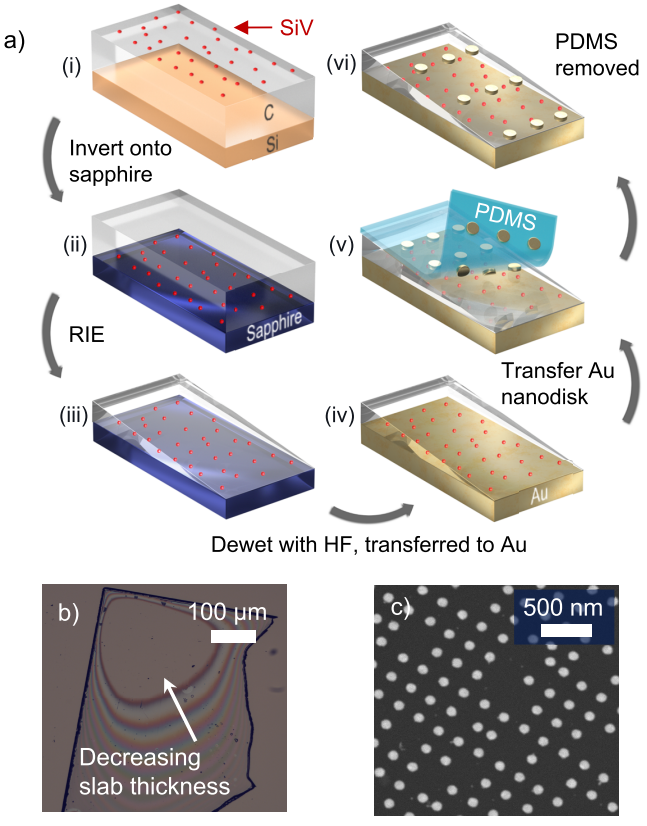

Figure 1. Sample fabrication overview. (a) Fabrication process for creating nanogap cavities with embedded SiVs. (b) Optical microscope image of the etched diamond slab after transfer onto a gold film. (c) SEM image of gold nanodisks after EBL fabrication on silicon.

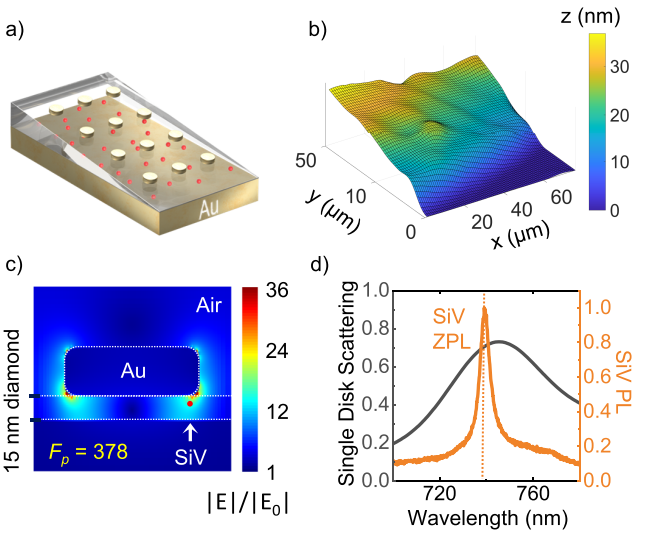

Figure 2. Approach for integration of SiVs in diamond into plasmonic nanogap cavities. (a) Schematic of sample structure consisting of Au nanodisks (30 nm height and 95 nm diameter) separated from an Au ground plane by an etched diamond slab. (b) Height profile of the thinnest part of the diamond slab measured using an imaging ellipsometer, with minimum thickness ∼10−20 nm (c) Electric field profile of the structure simulated via finite-difference, time-domain methods using a 738 nm normal incident plane wave (see SI). (d) Single disk scattering spectrum (black) overlaid with a PL spectrum of embedded SiVs (orange), showing good spectral overlap.

The plasmonic nanogap cavities possess a large electric field enhancement shown in Figure 2c, where the embedded SiVs are located at either a 5 or 10 nm targeted distance above the ground plane. The cavity resonance wavelength is determined by the geometry, material, and refractive index of the constituent nanogap cavity elements,[30−33] and here was chosen to match the SiV zero phonon line (ZPL) wavelength of 738 nm using a cavity formed by the Au ground plane and Au nanoparticles with a diameter of 95 nm and a height of 30 nm. The radiation pattern of the cavity structure has previously been shown to produce a single lobe normal to the surface, which generally improves the system's collection efficiency as compared to uncoupled emitters.[19,32] Here, we expect similar results for the radiation pattern, with a small modification due to the higher refractive index from diamond. The cavity was designed to overlap spectrally with the SiV emission in order to mainly enhance the spontaneous emission rate of the embedded SiVs, and only to a lesser extent the absorption rate.[34] A Purcell factor of 378 (120) is predicted at a depth of 10 nm (5 nm) above the ground plane for optimally positioned emitters near the cavity edge (simulations in SI).

Photoluminescence (PL) from cavity-coupled SiVs, as well as the plasmon resonance measured using white light scattering from single disks, are shown in Figure 2d, indicating their spectral overlap. The two implantation depths are studied to explore their effect on SiV lifetime and brightness. Further, two

https://doi.org/10.1021/acs.nanolett.3c04002
Nano Lett. 2024, 24, 3575−3580

cavity fill fractions—single cavity (4 μm spacing between elements) and metasurface (100 nm spacing between elements)—are fabricated for the 10 nm depth SiVs.

Time-resolved PL measurements are performed to determine the lifetime reduction achieved by embedding SiVs in the nanogap cavities. SiVs are excited at 514 nm with the second harmonic of a femtosecond Ti:sapphire laser. The SiV ZPL fluorescence is first isolated by a narrow band-pass filter and a series of dichroic, short, and long pass filters, followed by measurements using a high-resolution single-photon avalanche diode and time-tagged using a time to digital converter (see SI). Representative time-resolved PL decay curves for cavity coupled SiVs at 5 and 10 nm above the ground plane, as well as control SiV luminescence from uncoupled emitters, are shown in Figure 3a. Measurements of over 15 locations on each cavity

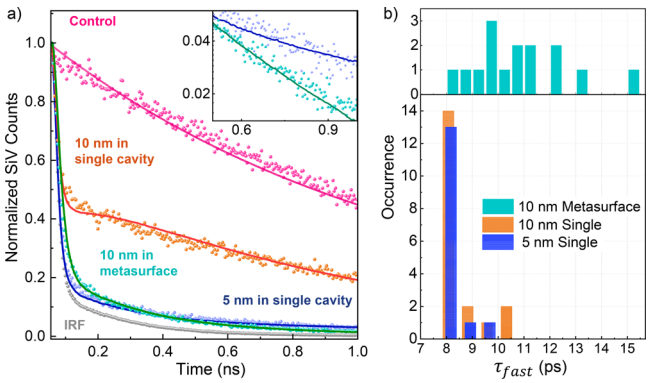

Figure 3. Time-resolved fluorescence lifetime from SiVs coupled to single nanocavities and a metasurface. (a) SiV lifetimes show biexponential decays from a single cavity (10 nm depth—orange, and 5 nm depth—blue) and 10 nm depth coupled to a metasurface (magenta). Lifetime for SiVs in diamond on silicon (control sample) exhibits similar single exponential decay (turquoise) for both depths, system IRF is displayed in gray. Inset: log plot highlighting the slow lifetime component of the 5 nm single cavity and 10 nm metasurface samples. (b) Histogram of τ_{fast} distribution for all three samples. Most spots from both single cavity samples exhibit $\tau_{fast} \leq 8$ ps, which is limited by the 4 ps bin size of the TCSPC system and is extracted via iterative reconvolution of a biexponential fit with the system IRF.

sample exhibit lifetime behaviors that can be well-described by biexponential decay fits, with an instrument-limited ultrafast response in the fast lifetime component (τ_{fast}).

Both the 5 and 10 nm implantation depth samples, with isolated single cavities, exhibit instrument-limited fast components of $\tau_{fast} \leq 8$ ps. The fast lifetimes are recovered through an iterative reconvolution technique using a least-squared method[35] with the measured instrument response function (IRF). The extracted lifetimes are limited by the 4 ps time bins of the time-correlated single photon counting (TCSPC) system, and in accordance with the Shannon–Nyquist theorem,[36,37] the fastest lifetime that can be extracted is 8 ps. Table 1 depicts the average fitted lifetime components reconvolved with the IRF for all samples. The control sample with a diamond membrane on a silicon substrate at both depths exhibits single exponential decays with an average lifetime of $\tau_{control}$ = 1.08 ± 0.05 ns. This is consistent with previously reported values for the SiV intrinsic lifetime,[1,38,39] though on the lower end of the reported range, likely because of the close proximity of the SiVs to the diamond surface.[26,40]

The integrated photon weight for single nanocavities τ_{fast}, *i.e.* area under the lifetime curve within the 80 MHz pulsed excitation, consists of 31 ± 3% and 10 ± 1% for the 5 and 10 nm SiV implantation depths samples, respectively. The experimental Purcell factor, Fp = 135, is found by dividing the average lifetime of SiVs in diamond on a silicon substrate (control sample) by the fast component of the lifetime of SiVs well-coupled to a nanogap cavity. In contrast, SiVs coupled to a metasurface of nanodisks display a slightly slower τ_{fast} = 10.7 ± 0.6 ps with a notably higher 63 ± 3% τ_{fast} contribution on average (Figure 3).

Next, PL intensity measurements are performed to study the brightness enhancement of SiVs in diamonds when embedded in single cavities. Figure 4a depicts the integrated PL counts/s

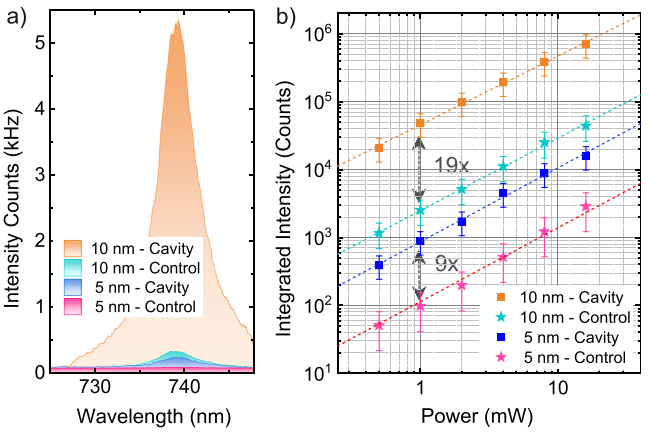

Figure 4. SiV PL power dependence of 10 and 5 nm implantation depth. (a) Example SiV intensity/s when SiVs are excited at 1 mW. (b) Integrated photon counts/s with 514 nm CW laser excitation from 0.5 mW to 16 mW on both sets of samples.

for the single cavity samples, for both 5 and 10 nm implantation depths, along with the control samples of diamond on Si, using 514 nm, 1 mW continuous wave excitation. The 10-nm-implantation-depth sample was brighter overall, with a 19-fold enhancement, compared to the 9-fold enhancement for the 5-nm-implantation-depth sample. Next, PL intensity is measured as a function of power, showing no signs of saturation at powers ≤ 16 mW. Notably, samples with SiVs implanted at 10 nm depth, both on Si and in the cavity, exhibited brighter emission than SiVs implanted at 5 nm either on Si or in the cavity. The dim PL of the 5 nm sample set can be attributed to the lower conversion efficiency of implanted

Table 1. Average Fitted Lifetimes for Plasmonic Nanogap Coupled SiVs and Control on Si

Sample	τ_{fast} (ps)	Contribution (%)	τ_{slow} (ps)	Contribution (%)
Si (5 and 10 nm)	-	-	1080 ± 50	-
5 nm—single cavity	≤8	31 ± 3	1000 ± 104	69 ± 3
10 nm—single cavity	≤8	10 ± 1	820 ± 81	90 ± 1
10 nm—metasurface	10.7 ± 0.6	63 ± 3	544 ± 26	37 ± 3

https://doi.org/10.1021/acs.nanolett.3c04002
Nano Lett. 2024, 24, 3575−3580

ions to SiVs, as well as nonradiative quenching from their respective ground plane.

Variations in lifetime and brightness between the two SiV depths can be explained by surface effects, as well as the depth distribution from the ion implantation. The SiVs closer to the ground plane experience less electric field enhancement, while the ones near the nanodisks experience a much higher enhancement. Further, with the implanted side of diamond contacting the Au ground plane, the emission from these SiVs is likely partially quenched by nonradiative pathways from the metal. The trends in Figure 3a and Figure 4b show good agreement: the nearly indistinguishable 5 nm depth lifetime from the IRF, and its low enhancement factor with significantly dimmer brightness compared to the 10 nm counterpart, suggest a presence of nonradiative decay pathways and/or poor implanted Si-ion-to-SiV conversion.

The observed biexponential lifetime can be attributed to the different degrees of coupling strength due to the combinations of emitters' lateral positions and depth distribution within the cavity. The lifetime statistic is composed of the emission from the well-coupled SiVs near the cavity edge (where maximum electric field enhancement occurs) and the poorly coupled SiVs within and surrounding the cavity. Notably, the τ_{fast} component from 10 nm depth SiVs integrated in a metasurface demonstrates a remarkably higher integrated photon count than that of a single cavity (Figure 3 and Table 1). We attribute this to the statistical distribution of SiV coupling strengths to the cavity: under the same collection area, regions surrounding single cavities consist mainly of uncoupled SiVs due to their 4 μm spacing, while metasurfaceswith tightly packed nanodisks results in a higher average degree of coupling. This can be further supported by its faster τ_{slow} as more SiVs are coupled to cavities under a metasurface. Similarly, when comparing single cavity studies for the 5 and 10 nm implantation-depth samples, the higher τ_{fast} contribution from the 5 nm samples likely arises from significant ground plane quenching as well as from fewer uncoupled SiVs surrounding the cavity due to the low conversion yield.[41]

In summary, ensemble SiVs embedded in thin-film diamond coupled to plasmonic nanogap cavities demonstrate up to 135-fold reduction in their fluorescence lifetime—more than an order of magnitude higher than previous demonstrations.[16,17] The SiVs are contained in single-crystal diamond films that have been etched down to nanometer-thin membranes. A dry-transfer technique of EBL-fabricated nanodisks printing is developed to integrate nanometer-thin diamond into plasmonic nanogaps while preserving its delicate nature. Emission from the nanogap cavity also yields a 19-fold brightness enhancement. However, the cavity resonance only overlaps with the emission spectrum, future design could target a cavity with a dual resonance to overlap both the SiV absorption and emission wavelengths in order to achieve an even brighter emission.[42]

Looking ahead, thin film diamond affords versatility as a functional layer for future integrated heterostructure stacks. Recently, fabrication of transferrable diamond films with tunable, uniform thickness down to 50 nm has been demonstrated.[43,44] A device that simultaneously hosts layers of superconducting, nonlinear, and/or photonic components could achieve advanced quantum state manipulation and open novel pathways toward a comprehensive device design for quantum information and sensing. Fabrication approaches such as laser annealing[45] could enable deterministic generation of cavity-coupled single photon sources in diamond. In addition, extreme Purcell enhancement from carefully engineered nanogap cavities could broaden an emitter's transform-limited line width and generate coherent, indistinguishable single photon emission at elevated temperatures.

■ ASSOCIATED CONTENT

Data Availability Statement

The data that support the plots within this paper and other findings of this study are available from the corresponding author upon reasonable request.

Supporting Information

The Supporting Information is available free of charge at https://pubs.acs.org/doi/10.1021/acs.nanolett.3c04002.

Additional lifetime analysis, position dependent Purcell factor simulation, cavity quality factor and mode volume, and additional experimental apparatus information. (PDF)

■ AUTHOR INFORMATION

Corresponding Author

Maiken H. Mikkelsen − *Department of Electrical and Computer Engineering, Duke University, Durham, North Carolina 27708, United States;* orcid.org/0000-0002-0487-7585; Email: m.mikkelsen@duke.edu

Authors

Andrew M. Boyce − *Department of Electrical and Computer Engineering, Duke University, Durham, North Carolina 27708, United States*

Hengming Li − *Department of Electrical and Computer Engineering, Duke University, Durham, North Carolina 27708, United States*

Nathaniel C. Wilson − *Department of Physics, Duke University, Durham, North Carolina 27708, United States*

Deniz Acil − *Department of Electrical and Computer Engineering, Duke University, Durham, North Carolina 27708, United States*

Amirhassan Shams-Ansari − *John A. Paulson School of Engineering and Applied Sciences, Harvard University, Cambridge, Massachusetts 02138, United States*

Srivatsa Chakravarthi − *Department of Physics, University of Washington, Seattle, Washington 98195, United States*

Christian Pederson − *Department of Physics, University of Washington, Seattle, Washington 98195, United States*

Qixin Shen − *Department of Physics, Duke University, Durham, North Carolina 27708, United States*

Nicholas Yama − *Department of Electrical and Computer Engineering, University of Washington, Seattle, Washington 98195, United States;* orcid.org/0000-0002-6123-3313

Kai-Mei C. Fu − *Department of Physics, University of Washington, Seattle, Washington 98195, United States; Department of Electrical and Computer Engineering, University of Washington, Seattle, Washington 98195, United States*

Marko Loncar − *John A. Paulson School of Engineering and Applied Sciences, Harvard University, Cambridge, Massachusetts 02138, United States*

Complete contact information is available at: https://pubs.acs.org/10.1021/acs.nanolett.3c04002

https://doi.org/10.1021/acs.nanolett.3c04002
Nano Lett. 2024, 24, 3575−3580

Author Contributions

†A.M.B., H.L., and N.C.W. contributed equally to this work

Notes

The authors declare no competing financial interest.

■ ACKNOWLEDGMENTS

The authors would like to acknowledge Arash Mirhamed at Accurion GmbH for performing imaging ellipsometry measurements on the sample and Stefan Bogdanovic for assistance in early stage lifetime measurements. This work is supported by an EFRI award from the National Science Foundation (NSF) (Award # 1640986). M.H.M. acknowledges support from AFOSR Award # FA9550-21-1-0312. H.L. acknowledges support from a National Science Foundation Graduate Research Fellowship. This work was performed in part using instrumentation at the Duke University Shared Materials Instrumentation Facility (SMIF). SMIF is a member of the North Carolina Research Triangle Nanotechnology Network (RTNN), which is supported by the National Science Foundation (Grant ECCS-1542015), as part of the National Nanotechnology Coordinated Infrastructure (NNCI). This work was also performed in part at the Harvard Center for Nanoscale Systems (CNS), a member of the NNCI, which is supported by the National Science Foundation (Grant ECCS-2025158).

■ REFERENCES

(1) Sipahigil, A.; Jahnke, K. D.; Rogers, L. J.; Teraji, T.; Isoya, J.; Zibrov, A. S.; Jelezko, F.; Lukin, M. D. Indistinguishable Photons from Separated Silicon-Vacancy Centers in Diamond. *Phys. Rev. Lett.* **2014**, *113* (11), 113602.

(2) Somaschi, N.; Giesz, V.; De Santis, L.; Loredo, J. C.; Almeida, M. P.; Hornecker, G.; Portalupi, S. L.; Grange, T.; Antón, C.; Demory, J.; Gómez, C.; Sagnes, I.; Lanzillotti-Kimura, N. D.; Lemaítre, A.; Auffeves, A.; White, A. G.; Lanco, L.; Senellart, P. Near-Optimal Single-Photon Sources in the Solid State. *Nat. Photonics* **2016**, *10* (5), 340−345.

(3) Huber, D.; Reindl, M.; Huo, Y.; Huang, H.; Wildmann, J. S.; Schmidt, O. G.; Rastelli, A.; Trotta, R. Highly Indistinguishable and Strongly Entangled Photons from Symmetric GaAs Quantum Dots. *Nat. Commun.* **2017**, *8* (1), 15506.

(4) Sun, S.; Kim, H.; Luo, Z.; Solomon, G. S.; Waks, E. A Single-Photon Switch and Transistor Enabled by a Solid-State Quantum Memory. *J. Phys. B At. Mol. Opt. Phys.* **2018**, *361* (6397), 57−60.

(5) Sukachev, D. D.; Sipahigil, A.; Nguyen, C. T.; Bhaskar, M. K.; Evans, R. E.; Jelezko, F.; Lukin, M. D. Silicon-Vacancy Spin Qubit in Diamond: A Quantum Memory Exceeding 10 Ms with Single-Shot State Readout. *Phys. Rev. Lett.* **2017**, *119* (22), 223602.

(6) Serrano, D.; Karlsson, J.; Fossati, A.; Ferrier, A.; Goldner, P. All-Optical Control of Long-Lived Nuclear Spins in Rare-Earth Doped Nanoparticles. *Nat. Commun.* **2018**, *9* (1), 2127.

(7) Carter, S. G.; Sweeney, T. M.; Kim, M.; Kim, C. S.; Solenov, D.; Economou, S. E.; Reinecke, T. L.; Yang, L.; Bracker, A. S.; Gammon, D. Quantum Control of a Spin Qubit Coupled to a Photonic Crystal Cavity. *Nat. Photonics* **2013**, *7* (4), 329−334.

(8) Neumann, P.; Jakobi, I.; Dolde, F.; Burk, C.; Reuter, R.; Waldherr, G.; Honert, J.; Wolf, T.; Brunner, A.; Shim, J. H.; Suter, D.; Sumiya, H.; Isoya, J.; Wrachtrup, J. High-Precision Nanoscale Temperature Sensing Using Single Defects in Diamond. *Nano Lett.* **2013**, *13* (6), 2738−2742.

(9) Clevenson, H.; Trusheim, M. E.; Teale, C.; Schröder, T.; Braje, D.; Englund, D. Broadband Magnetometry and Temperature Sensing with a Light-Trapping Diamond Waveguide. *Nat. Phys.* **2015**, *11* (5), 393−397.

(10) Trusheim, M. E.; Englund, D. Wide-Field Strain Imaging with Preferentially Aligned Nitrogen-Vacancy Centers in Polycrystalline Diamond. *New J. Phys.* **2016**, *18* (12), 123023.

(11) Acosta, V. M.; Jensen, K.; Santori, C.; Budker, D.; Beausoleil, R. G. Electromagnetically Induced Transparency in a Diamond Spin Ensemble Enables All-Optical Electromagnetic Field Sensing. *Phys. Rev. Lett.* **2013**, *110* (21), 213605.

(12) Wolfowicz, G.; Whiteley, S. J.; Awschalom, D. D. Electrometry by Optical Charge Conversion of Deep Defects in 4H-SiC. *Proc. Natl. Acad. Sci. U. S. A.* **2018**, *115* (31), 7879−7883.

(13) Bradac, C.; Gao, W.; Forneris, J.; Trusheim, M. E.; Aharonovich, I. Quantum Nanophotonics with Group IV Defects in Diamond. *Nat. Commun.* **2019**, *10* (1), 5625.

(14) Pelton, M. Modified Spontaneous Emission in Nanophotonic Structures. *Nat. Photonics* **2015**, *9* (7), 427−435.

(15) Hausmann, B. J. M.; Shields, B. J.; Quan, Q.; Chu, Y.; De Leon, N. P.; Evans, R.; Burek, M. J.; Zibrov, A. S.; Markham, M.; Twitchen, D. J.; Park, H.; Lukin, M. D.; Lončar, M. Coupling of NV Centers to Photonic Crystal Nanobeams in Diamond. *Nano Lett.* **2013**, *13* (12), 5791−5796.

(16) Riedrich-Möller, J.; Arend, C.; Pauly, C.; Mücklich, F.; Fischer, M.; Gsell, S.; Schreck, M.; Becher, C. Deterministic Coupling of a Single Silicon-Vacancy Color Center to a Photonic Crystal Cavity in Diamond. *Nano Lett.* **2014**, *14* (9), 5281−5287.

(17) Zhang, J. L.; Sun, S.; Burek, M. J.; Dory, C.; Tzeng, Y. K.; Fischer, K. A.; Kelaita, Y.; Lagoudakis, K. G.; Radulaski, M.; Shen, Z. X.; Melosh, N. A.; Chu, S.; Lončar, M.; Vučković, J. Strongly Cavity-Enhanced Spontaneous Emission from Silicon-Vacancy Centers in Diamond. *Nano Lett.* **2018**, *18* (2), 1360−1365.

(18) Benedikter, J.; Kaupp, H.; Hümmer, T.; Liang, Y.; Bommer, A.; Becher, C.; Krueger, A.; Smith, J. M.; Hänsch, T. W.; Hunger, D. Cavity-Enhanced Single-Photon Source Based on the Silicon-Vacancy Center in Diamond. *Phys. Rev. Appl.* **2017**, *7* (2), 024031.

(19) Bogdanov, S. I.; Shalaginov, M. Y.; Lagutchev, A. S.; Chiang, C. C.; Shah, D.; Baburin, A. S.; Ryzhikov, I. A.; Rodionov, I. A.; Kildishev, A. V.; Boltasseva, A.; Shalaev, V. M. Ultrabright Room-Temperature Sub-Nanosecond Emission from Single Nitrogen-Vacancy Centers Coupled to Nanopatch Antennas. *Nano Lett.* **2018**, *18* (8), 4837−4844.

(20) Rondin, L.; Dantelle, G.; Slablab, A.; Grosshans, F.; Treussart, F.; Bergonzo, P.; Perruchas, S.; Gacoin, T.; Chaigneau, M.; Chang, H. C.; Jacques, V.; Roch, J. F. Surface-Induced Charge State Conversion of Nitrogen-Vacancy Defects in Nanodiamonds. *Phys. Rev. B* **2010**, *82* (11), 115449.

(21) Wolters, J.; Sadzak, N.; Schell, A. W.; Schröder, T.; Benson, O. Measurement of the Ultrafast Spectral Diffusion of the Optical Transition of Nitrogen Vacancy Centers in Nano-Size Diamond Using Correlation Interferometry. *Phys. Rev. Lett.* **2013**, *110* (2), 027401.

(22) Laraoui, A.; Hodges, J. S.; Meriles, C. A. Nitrogen-Vacancy-Assisted Magnetometry of Paramagnetic Centers in an Individual Diamond Nanocrystal. *Nano Lett.* **2012**, *12* (7), 3477−3482.

(23) Lagomarsino, S.; Flatae, A. M.; Kambalathmana, H.; Sledz, F.; Hunold, L.; Soltani, N.; Reuschel, P.; Sciortino, S.; Gelli, N.; Massi, M.; Czelusniak, C.; Giuntini, L.; Agio, M. Creation of Silicon-Vacancy Color Centers in Diamond by Ion Implantation. *Front. Phys.* **2021**, *8*, 8.

(24) Santori, C.; Barclay, P. E.; Fu, K. M. C.; Beausoleil, R. G. Vertical Distribution of Nitrogen-Vacancy Centers in Diamond Formed by Ion Implantation and Annealing. *Phys. Rev. B* **2009**, *79* (12), 125313.

(25) Grosso, G.; Moon, H.; Lienhard, B.; Ali, S.; Efetov, D. K.; Furchi, M. M.; Jarillo-Herrero, P.; Ford, M. J.; Aharonovich, I.; Englund, D. Tunable and High-Purity Room Temperature Single-Photon Emission from Atomic Defects in Hexagonal Boron Nitride. *Nat. Commun.* **2017**, *8* (1), 705.

(26) Evans, R. E.; Bhaskar, M. K.; Sukachev, D. D.; Nguyen, C. T.; Sipahigil, A.; Burek, M. J.; Machielse, B.; Zhang, G. H.; Zibrov, A. S.; Bielejec, E.; Park, H.; Lončar, M.; Lukin, M. D. Photon-Mediated

https://doi.org/10.1021/acs.nanolett.3c04002
Nano Lett. 2024, 24, 3575−3580

Interactions between Quantum Emitters in a Diamond Nanocavity. *Science* **2018**, *362* (6415), 662−665.
(27) Gould, M.; Chakravarthi, S.; Christen, I. R.; Thomas, N.; Dadgostar, S.; Song, Y.; Lee, M. L.; Hatami, F.; Fu, K.-M. C. Large-Scale GaP-on-Diamond Integrated Photonics Platform for NV Center-Based Quantum Information. *J. Opt. Soc. Am. B* **2016**, *33* (3), B35−B42.
(28) Nguyen, C. T.; Sukachev, D. D.; Bhaskar, M. K.; MacHielse, B.; Levonian, D. S.; Knall, E. N.; Stroganov, P.; Chia, C.; Burek, M. J.; Riedinger, R.; Park, H.; Lončar, M.; Lukin, M. D. An Integrated Nanophotonic Quantum Register Based on Silicon-Vacancy Spins in Diamond. *Phys. Rev. B* **2019**, *100* (16), 165428.
(29) Chia, C.; Machielse, B.; Shams-Ansari, A.; Lončar, M. Development of Hard Masks for Reactive Ion Beam Angled Etching of Diamond. *Opt. Express* **2022**, *30* (9), 14189.
(30) Moreau, A.; Ciracì, C.; Mock, J. J.; Smith, D. R.; Hill, R. T.; Chilkoti, A.; Wang, Q.; Wiley, B. J. Controlled-Reflectance Surfaces with Film-Coupled Colloidal Nanoantennas. *Nature* **2012**, *492* (7427), 86−89.
(31) Lassiter, J. B.; McGuire, F.; Mock, J. J.; Ciraci, C.; Hill, R. T.; Wiley, B. J.; Chilkoti, A.; Smith, D. R. Plasmonic Waveguide Modes of Film-Coupled Metallic Nanocubes. *Nano Lett.* **2013**, *13* (12), 5866−5872.
(32) Chikkaraddy, R.; Zheng, X.; Benz, F.; Brooks, L. J.; De Nijs, B.; Carnegie, C.; Kleemann, M. E.; Mertens, J.; Bowman, R. W.; Vandenbosch, G. A. E.; Moshchalkov, V. V.; Baumberg, J. J. How Ultranarrow Gap Symmetries Control Plasmonic Nanocavity Modes: From Cubes to Spheres in the Nanoparticle-on-Mirror. *ACS Photonics* **2017**, *4* (3), 469−475.
(33) Akselrod, G. M.; Huang, J.; Hoang, T. B.; Bowen, P. T.; Su, L.; Smith, D. R.; Mikkelsen, M. H. Large-Area Metasurface Perfect Absorbers from Visible to Near-Infrared. *Adv. Mater.* **2015**, *27* (48), 8028−8034.
(34) Purcell, E. M. Spontaneous Emission Probabilities at Radio Frequencies. *Phys. Rev.* **1946**, *69*, 246−260.
(35) Enderlein, J.; Erdmann, R. Fast Fitting of Multi-Exponential Decay Curves. *Opt. Commun.* **1997**, *134* (1−6), 371−378.
(36) Wahl, M. Time-Correlated Single Photon Counting. *Time-Correlated Single Photon Counting*; PicoQuant GmbH: Berlin, 2017; p 5.
(37) Becker, W. In *Advanced Time-Correlated Single Photon Counting Techniques*; Castleman, A. W., Jr., Toennies, J. P., Zinth, W., Eds.; Springer, 2005.
(38) Jahnke, K. D.; Sipahigil, A.; Binder, J. M.; Doherty, M. W.; Metsch, M.; Rogers, L. J.; Manson, N. B.; Lukin, M. D.; Jelezko, F. Electron-Phonon Processes of the Silicon-Vacancy Centre in Diamond. *New J. Phys.* **2015**, *17*, 043011.
(39) Leifgen, M.; Schröder, T.; Gädeke, F.; Riemann, R.; Métillon, V.; Neu, E.; Hepp, C.; Arend, C.; Becher, C.; Lauritsen, K.; Benson, O. Evaluation of Nitrogen- and Silicon-Vacancy Defect Centres as Single Photon Sources in Quantum Key Distribution. *New J. Phys.* **2014**, *16*, 023021.
(40) Evans, R. E.; Sipahigil, A.; Sukachev, D. D.; Zibrov, A. S.; Lukin, M. D. Narrow-Linewidth Homogeneous Optical Emitters in Diamond Nanostructures via Silicon Ion Implantation. *Phys. Rev. Appl.* **2016**, *5* (4). DOI: 10.1103/PhysRevApplied.5.044010.
(41) Pezzagna, S.; Naydenov, B.; Jelezko, F.; Wrachtrup, J.; Meijer, J. Creation Efficiency of Nitrogen-Vacancy Centres in Diamond. *New J. Phys.* **2010**, *12*, 065017.
(42) Shen, Q.; Shams-Ansari, A.; Boyce, A. M.; Wilson, N. C.; Cai, T.; Loncar, M.; Mikkelsen, M. H. A Metasurface-Based Diamond Frequency Converter Using Plasmonic Nanogap Resonators. *Nanophotonics* **2020**, *10* (1), 589−595.
(43) Guo, X.; Delegan, N.; Karsch, J. C.; Li, Z.; Liu, T.; Shreiner, R.; Butcher, A.; Awschalom, D. D.; Heremans, F. J.; High, A. A. Tunable and Transferable Diamond Membranes for Integrated Quantum Technologies. *Nano Lett.* **2021**, *21* (24), 10392−10399.
(44) Guo, X.; Xie, M.; Addhya, A.; Linder, A.; Zvi, U.; Deshmukh, T. D.; Liu, Y.; Hammock, I. N.; Li, Z.; DeVault, C. T.; Butcher, A.; Esser-Kahn, A. P.; Awschalom, D. D.; Delegan, N.; Maurer, P. C.; Heremans, F. J.; High, A. A. Direct-Bonded Diamond Membranes for Heterogeneous Quantum and Electronic Technologies. *arXiv* **2023**, 2306.04408.
(45) Chen, Y.-C.; Griffiths, B.; Weng, L.; Nicley, S. S.; Ishmael, S. N.; Lekhai, Y.; Johnson, S.; Stephen, C. J.; Green, B. L.; Morley, G. W.; Newton, M. E.; Booth, M. J.; Salter, P. S.; Smith, J. M. Laser Writing of Individual Nitrogen-Vacancy Defects in Diamond with near-Unity Yield. *Optica* **2019**, *6* (5), 662.

https://doi.org/10.1021/acs.nanolett.3c04002
Nano Lett. 2024, 24, 3575−3580